

## RUNAWAY STARS AND THE ESCAPE OF IONIZING RADIATION FROM HIGH-REDSHIFT GALAXIES

CHARLIE CONROY & KAITLIN M. KRATTER  
Harvard-Smithsonian Center for Astrophysics, Cambridge, MA, USA  
*Draft version May 17, 2012*

### ABSTRACT

Approximately 30% of all massive stars in the Galaxy are runaways with velocities exceeding  $30 \text{ km s}^{-1}$ . Their high speeds allow them to travel  $\sim 0.1 - 1 \text{ kpc}$  away from their birth place before they explode at the end of their several Myr lifetimes. At high redshift, when galaxies were much smaller than in the local universe, runaways could venture far from the dense inner regions of their host galaxies. From these large radii, and therefore low column densities, much of their ionizing radiation is able to escape into the intergalactic medium. Runaways may therefore significantly enhance the overall escape fraction of ionizing radiation,  $f_{\text{esc}}$ , from small galaxies at high redshift. We present simple models of the high-redshift runaway population and its impact on  $f_{\text{esc}}$  as a function of halo mass, size, and redshift. We find that the inclusion of runaways enhances  $f_{\text{esc}}$  by factors of  $\approx 1.1 - 8$ , depending on halo mass, galaxy geometry, and the mechanism of runaway production, implying that runaways may contribute 50–90% of the total ionizing radiation escaping from high-redshift galaxies. Runaways may therefore play an important role in reionizing the universe.

*Subject headings:* reionization — galaxies: high-redshift

### 1. INTRODUCTION

Observations of the cosmic microwave background (Dunkley et al. 2009; Komatsu et al. 2011) and the absorption spectra of high-redshift quasars (Fan et al. 2006) imply that the universe was reionized sometime between  $6 < z < 12$ . The rapid drop in the quasar luminosity function at high redshift suggests that massive stars provide the bulk of the ionizing luminosity responsible for reionization (Madau et al. 1999; Loeb & Barkana 2001; Bolton et al. 2005). Stars at high redshift are born within dense proto-galactic fragments, and thus much of their ionizing luminosity is thought to be attenuated by neutral hydrogen. The fraction of their ionizing luminosity that escapes into the intergalactic medium (IGM) and is available to reionize the universe,  $f_{\text{esc}}$ , is a key quantity in determining how reionization occurred.

Models for reionization that reproduce the observed UV luminosity function of high-redshift galaxies require both  $f_{\text{esc}} \gtrsim 0.1$  and significant contributions from very faint galaxies (e.g., Pawlik et al. 2009; Srbinovsky & Wythe 2010; Haardt & Madau 2012; Kuhlen & Faucher-Giguere 2012; Bouwens et al. 2011a). These requirements place very demanding constraints on models of high-redshift galaxies.

In the local universe, observations of both normal star forming and starburst galaxies favor escape fractions in the range of a few percent (Leitherer et al. 1995; Bland-Hawthorn & Maloney 1999; Heckman et al. 2001; Grimes et al. 2007). The escape fraction seems to be similarly low at  $z \sim 1$  (Siana et al. 2007; Cowie et al. 2009; Siana et al. 2010). At higher redshifts ( $z \sim 3$ ), observations suggest that  $f_{\text{esc}}$  may increase to  $\sim 10\%$ , at least for the relatively massive, highly star-forming galaxies for which measurements of  $f_{\text{esc}}$  have been made (Steidel et al. 2001; Giallongo et al. 2002; Shapley et al. 2006; Inoue et al. 2006; Siana et al. 2007; Iwata et al. 2009; Siana et al. 2010). However, constraints on  $f_{\text{esc}}$  at  $z > 2$  from gamma-ray burst afterglows favor low values of  $f_{\text{esc}} \approx 0.02$  (Chen et al. 2007). While the data suggest that escape fractions may increase out to  $z \sim 3$ , it is worth noting that direct measurements of ionizing photons during the epoch of reionization are impossi-

ble, owing to the high opacity of the IGM. Our understanding of how reionization proceeded therefore depends crucially on models and simulations that follow the escape of ionizing photons.

Simple theoretical estimates of  $f_{\text{esc}}$  can be obtained from analytic models of galaxies and HII regions (Dove & Shull 1994; Haiman & Loeb 1997; Madau et al. 1999; Dove et al. 2000; Ricotti & Shull 2000; Wood & Loeb 2000; Fernandez & Shull 2011). These models produce estimates of  $f_{\text{esc}}$  that vary widely from  $10^{-3}$  to  $\sim 1$  depending on dark matter halo mass, clumpiness of the interstellar medium (ISM), gas density profile, and redshift. Sophisticated hydrodynamical simulations also predict a wide range of escape fractions (Razoumov & Sommer-Larsen 2006, 2007; Gnedin et al. 2008; Wise & Cen 2009; Razoumov & Sommer-Larsen 2010; Yajima et al. 2011).

While some of the differences between model predictions can be attributed to different choices for physical parameters such as halo mass and redshift, numerical methods and sub-grid models also contribute to the quoted discrepancies. For example, the geometry of the ISM and the relative distribution of stars and gas has a strong influence of  $f_{\text{esc}}$ , and both are controlled by uncertain prescriptions for star formation and supernovae feedback. Clarke & Oey (2002) argued that there is a critical star formation rate above which the porosity of the ISM is approximately unity. A highly porous ISM is expected to result in a high escape fraction (Fujita et al. 2003). Indeed, simulations are able to achieve high escape fractions only when stellar feedback is very strong and hence the porosity is very high. Ricotti (2002) has considered globular clusters as efficient sources of ionizing photons due to their high star formation efficiencies and high porosities. In this paper we consider an alternative scenario that is capable of producing very high escape fractions without appealing to a highly porous ISM: the contribution from runaway stars.

A significant fraction of massive stars in the Galaxy are moving at high velocity ( $> 30 \text{ km s}^{-1}$ ) and are therefore known as runaways (e.g., Blaauw 1961; Gies & Bolton 1986). Two formation channels have been proposed for the formation

of runaways: 1) via dynamical ejections from young dense stellar systems (Gies & Bolton 1986; Fujii & Portegies Zwart 2011; Perets & Subr 2012), and 2) due to the explosion of a companion star (Zwicky 1957; Blaauw 1961; Gott et al. 1970; Portegies Zwart 2000; Eldridge et al. 2011). A combination of these two scenarios has also been considered (Pflamm-Altenburg & Kroupa 2010). Tracing the orbits of runaways back in time has provided evidence that both channels contribute to the runaway population (Hoogerwerf et al. 2001). The available data on runaways allow for a wide range in the fraction of massive stars that are runaways,  $f_{\text{run}}$ , from 0.1–0.5 depending on definition and correction for completeness and observational biases (e.g., Gies & Bolton 1986; Gies 1987; Stone 1991; Tetzlaff et al. 2011).

The goal of this paper is to assess the effect of runaways on the escape of ionizing radiation from high-redshift galaxies. Qualitatively we expect them to be important when galaxy sizes are smaller than  $\sim 100$  pc, as then even relatively slow runaways with short main sequence lifetimes can travel from a galaxy’s center to its outskirts before exploding. In this paper we will explore the effect of runaways by building simple analytic models of high-redshift galaxies and modeling runaways formed through both the dynamical and supernova mechanisms. The potential importance of runaway stars on the escape of ionizing photons was first noted by Dove & Shull (1994) in the context of the Galaxy.

Throughout this paper we adopt cosmological parameters consistent with the 7th year *WMAP* estimates (Komatsu et al. 2011), namely  $\Omega_{\Lambda} = 0.73$  and  $\Omega_m = 0.27$ , and a Hubble constant of  $H_0 = 70 \text{ km s}^{-1} \text{ Mpc}^{-1}$ .

## 2. MODEL

Our goal is to construct simple models for the escape fraction of ionizing radiation from high-redshift galaxies both with and without the contribution of runaways. Our basic setup is motivated by and follows the approach of Ricotti & Shull (2000), and references therein.

### 2.1. Galaxy Models

We begin by considering the relation between cold dark matter halo mass and virial radius derived from cosmological  $N$ -body simulations (Navarro et al. 1997):

$$r_{\text{vir}} = 0.96 \text{ kpc} \left( \frac{M_{\text{halo}}}{10^8 M_{\odot}} \right)^{1/3} \left( \frac{\Omega_m}{\Omega_m(z)} \frac{\Delta_c}{200} \right)^{-1/3} \left( \frac{1+z}{10} \right)^{-1}, \quad (1)$$

where  $\Omega_m$  and  $\Omega_m(z)$  are the matter densities of the universe at the present epoch and redshift  $z$ , respectively, in units of the critical density ( $\rho_{\text{crit}} = 3H_0^2/8/\pi G$ ), and  $\Delta_c$  is the overdensity threshold of virialized dark matter halos, which depends on  $\Omega_m(z)$  (Bryan & Norman 1998). For our fiducial model we adopt  $z = 10$ .

We will assume that 100% of the baryons are in the cold gas phase (i.e., the stellar fraction is  $\approx 0$  at these early epochs; see e.g., Ricotti et al. 2002; Wise & Cen 2009), implying:

$$M_{\text{gas}} = f_b M_{\text{halo}}, \quad (2)$$

where  $f_b = 0.17$  is the universal baryon fraction (Komatsu et al. 2011). The relation between the gas scale radius and the halo virial radius is taken to be (Mo et al. 1998):

$$r_g = \frac{j_d \lambda}{\sqrt{2} f_b} r_{\text{vir}}, \quad (3)$$

where  $\lambda$  is the dimensionless spin parameter, which for halos in simulations has a mean value of 0.04 (Bullock et al. 2001). The galaxy angular momentum is a fraction  $j_d$  of that of the halo. We assume  $j_d/f_b = 1$  and  $\lambda = 0.05$ , as these parameters provide a good fit to the observed size distribution of local galactic disks (Mo et al. 1998).

High-resolution cosmological hydrodynamic simulations produce a wide range of galaxy morphologies at high redshift, ranging from spherical to well-ordered disks (Wise & Cen 2009; Pawlik et al. 2011; Romano-Díaz et al. 2011; Wise et al. 2012). Because the true nature of these galaxies remains unknown, and at present unobservable, we consider two galaxy geometries, spherical and disk-like. In our spherical model the gas has an exponential number density profile,  $n(r) = n_0 e^{-r/r_g}$ . In our disk model, we consider a gas profile with  $n(r, z) = n_0 e^{-R/r_g} e^{-z^2/z_g^2}$ , where  $z_g$  is the disk scale height. We consider models where the disk height-to-disk scale length ratio varies with mass as:

$$\frac{z_g}{r_g} = 0.2 \left( \frac{M_{\text{halo}}}{10^8 M_{\odot}} \right)^{-2/3}. \quad (4)$$

The mass dependence of  $z_g/r_g$  follows from the assumption of an isothermal disk (e.g., Wood & Loeb 2000). To ensure that  $z_g/r_g$  never exceeds unity we sum its inverse in quadrature with one:  $(z_g/r_g)^{-2} \rightarrow (z_g/r_g)^{-2} + 1$ .

In our fiducial model massive stars and stellar clusters are born tracing the gas density profile. We will also consider a model where the stellar density is proportional to the gas density squared ( $\rho_* \propto \rho_g^2$ ) as in Wood & Loeb (2000). The slope of the observed Kennicutt-Schmidt relation between star formation rate surface density and gas surface density falls in between these two extremes (Kennicutt 1998). The gas and stellar density distributions are truncated at  $5r_g = 0.2r_{\text{vir}}$  (and  $5z_g$  for disks). In summary, for our fiducial set of model parameters, the halo mass uniquely specifies the distribution of gas and stars within the halo.

### 2.2. Photon Escape Fraction

Our next task is to compute  $f_{\text{esc}}$ . As discussed in Dove & Shull (1994) and Ricotti & Shull (2000), the HII regions created by massive stars will not be spherical if the local gradient in the gas density profile is large. While the HII regions are allowed to be non-spherical in our model, the equations presented in this section assume that the gas distribution is spherical; the generalization to disk geometries is straightforward. Consider a star a distance  $r$  from the center of the galaxy. A point residing a distance  $r'$  from the star at an angle  $\theta$  from the line connecting the galaxy center and the star will be at a distance  $R = \sqrt{r^2 + r'^2 + 2rr'\cos\theta}$  from the center of the galaxy (see Figure 1 in Ricotti & Shull 2000, for a sketch of the geometrical configuration)<sup>1</sup>. At each angle  $\theta$  one can compute the quantity:

$$f(\theta) = 1 - \frac{4\pi\alpha_H^B}{Q} \int_0^\infty n_H(R)^2 r'^2 dr', \quad (5)$$

where  $Q \equiv Q_H$  is the hydrogen ionizing luminosity,  $\alpha_H^B$  is the hydrogen case B recombination coefficient, and  $n_H$  is the number density of hydrogen. We adopt  $\alpha_H^B = 2.6 \times$

<sup>1</sup> There appears to be an erroneous substitution of sin for cos in their equation for  $R$ .

$10^{-13} \text{ cm}^{-3} \text{ s}^{-1}$ , appropriate for gas at  $T = 10^4 \text{ K}$ . Values of  $f > 0$  indicate a non-zero escape fraction, while  $f \leq 0$  indicates that 100% of the ionizing radiation is absorbed. The critical angle for escape,  $\theta_c$  is defined through the equation  $f(\theta_c) = 0.0$ . Notice that  $\theta_c$  is a function of  $Q$  and  $r$ . The angle-averaged fraction of ionizing photons escaping the galaxy is then computed by integrating  $f(\theta)$  over a solid angle:

$$\langle f_{\text{esc}} \rangle = \frac{1}{4\pi} \int_0^{\theta_c} f(\theta) 2\pi \sin \theta d\theta. \quad (6)$$

The total escape fraction of the galaxy is then computed by integrating over  $r$  and  $Q$ :

$$f_{\text{esc}} = \int \int \langle f_{\text{esc}} \rangle P(r) P(Q) dr dQ, \quad (7)$$

where  $P(r)$  and  $P(Q)$  are the probabilities of a star being at location  $r$  and with ionizing luminosity  $Q$ .

We have neglected the effect of overlapping HII regions in our analytic framework. This is a common simplification made in the modeling of the ionizing escape fraction (Dove & Shull 1994; Ricotti & Shull 2000). The effect of including HII overlap would be to increase  $f_{\text{esc}}$ , although the low expected star formation rates in  $z = 10$  halos (Wise & Cen 2009) suggests that HII overlap may not be significant.

In the absence of runaways,  $P(r)$  and  $P(Q)$  are straightforward to specify (our prescription for including runaways is described in §2.3). The former is determined by the gas density profile, while the latter is taken to be the observed ionizing luminosity function (LF) in local galaxies. The LFs of OB associations in nearby galaxies have power-law indices that range between  $-1.5$  and  $-2.5$  over the range  $48 \lesssim \log(Q/s^{-1}) \lesssim 51$  (Kennicutt et al. 1989; McKee & Williams 1997; Whitmore et al. 1999; van Zee 2000; Azimlu et al. 2011). Oey & Clarke (1998) argued that the data are consistent with a universal power-law slope of  $-2.0$ . We therefore adopt an ionizing LF with a  $P(Q) \propto Q^{-2.0}$  over the range  $48 < \log(Q/s^{-1}) < 51$ . For reference,  $\log(Q) = 48$  corresponds to a single  $20 M_{\odot}$  star. We will explore variation in the lower luminosity cutoff,  $Q_{\text{min}}$ , in §3. Notice that our treatment of  $P(Q)$  naturally accounts for the fact that massive stars are clustered.

Current evidence favors very little if any dust in low mass galaxies at high redshift, as inferred from their very blue UV colors (Bouwens et al. 2011b). The lack of dust is also consistent with their expected low metallicities. Our fiducial model is therefore dust-free, but we nevertheless explore the effect of dust on  $f_{\text{esc}}$ . To incorporate dust into our models, we adopt a wavelength dependent dust cross section,  $\sigma(\lambda)$  from Pei (1992), as updated in Gnedin et al. (2008). Essentially nothing is known about the dust composition nor grain size distribution in high-redshift galaxies, so we consider both Large and Small Magellanic Cloud-type dust (LMC and SMC, respectively) to give a sense of the variation expected from different grain populations. To make the computations simple, we have taken averages of  $\sigma(\lambda)$  over ionizing photons, weighted by model stellar flux distributions from Smith et al. (2002). The average depends weakly on the effective temperature, varying by  $\sim 10\%$  over the relevant range. The resulting flux-weighted mean cross sections for LMC and SMC dust are  $\sigma = 1 \times 10^{-21} \text{ cm}^{-2}$  and  $\sigma = 5 \times 10^{-22} \text{ cm}^{-2}$ , respectively. For each  $r, \theta$  pair we can compute  $\tau_d = \sigma N_H$ , where  $N_H$  is the column density of hydrogen (we adopt the observed

dust-to-gas ratios of the LMC and SMC, which likely overestimates the influence of dust at high redshift). The hydrogen ionizing luminosity  $Q$  that enters into Equation 5 is then simply attenuated by  $e^{-\tau_d}$ .

With the gas density profile, ionizing LF, and dust model specified,  $f_{\text{esc}}$  for non-runaway stars is then uniquely determined as a function of halo mass. We now consider the addition of runaways.

### 2.3. Runaways

For the purposes of computing  $f_{\text{esc}}$ , runaways differ from non-runaways in two respects: they travel from their birth environment, resulting in a change to  $P(r)$ , and the runaway population may not reflect the overall massive star population in its mass distribution and therefore its ionizing LF. As noted in the Introduction, there are two mechanisms capable of producing runaways in the Galaxy: 1) dynamical encounters in young dense stellar systems, and 2) the explosion of a close companion. In order to explore the effects of runaways on  $f_{\text{esc}}$  we develop simple models for both scenarios, motivated by the observed runaway population in the local universe.

In the dynamical mechanism, runaways inherit a high velocity,  $V_{\text{run}}$ , not long after their birth. We model runaways produced via this mechanism by taking a fraction of all massive stars,  $f_{\text{run}}$ , and giving them a velocity  $V_{\text{run}}$  at birth with a random direction in the galaxy. The runaway is allowed to travel for a time equal to its main sequence lifetime. The effect of the potential due to the galaxy and halo mass on the motion of the runaways is neglected<sup>2</sup>.

In the simplest version of this model we assume that the runaways are, at birth, a random sampling of the overall massive star population. However, in reality one may expect the maximum mass of runaways produced in this mechanism to be lower than the upper mass of all stars. This may occur because dynamical encounters tend to eject the lowest mass star in the encounter (Anosova 1986). We model this effect by considering a possible truncation in stellar mass,  $M_{\text{max}}$ , of the runaway mass function.

We explore models where  $V_{\text{run}}$  either takes a single value or a distribution. The numerical models of Fujii & Portegies Zwart (2011) and Perets & Subr (2012) produce runaways with a power-law distribution of  $V_{\text{run}}$  with an index of  $\approx -1$  and  $\approx -1.5$ , respectively, over the range  $20 \text{ km s}^{-1} < V_{\text{run}} < 100 \text{ km s}^{-1}$ . Observations of runaways in the Galaxy seem to favor a Maxwellian velocity distribution with a dispersion of  $\approx 30 \text{ km s}^{-1}$  (Stone 1991; Tetzlaff et al. 2011), implying a mean runaway velocity of  $\approx 45 \text{ km s}^{-1}$ . We consider both of these distributions and their effects on  $f_{\text{esc}}$ .

For the dynamical model we assume that the runaway LF is equal to the non-runaway LF up to a maximum ionizing luminosity corresponding to a mass of  $100 M_{\odot}$ . Conceptually, this corresponds to replacing clusters with single stars. See the discussion in Oey & Clarke (1998), where they find that the single-star LF does not significantly differ from the cluster LF for a range of assumptions. To calculate the influence of runaways, we must translate a given luminosity into a stellar mass so that we may assign stellar lifetimes. We have constructed

<sup>2</sup> The circular velocity of dark matter halos at  $0.1 r_{\text{vir}} \approx 3 r_g$  is  $< 30 \text{ km s}^{-1}$  for  $M_{\text{halo}} < 10^9 M_{\odot}$  and  $< 60 \text{ km s}^{-1}$  for  $M_{\text{halo}} < 10^{10} M_{\odot}$  (Navarro et al. 1997). For the typical runaway velocities we consider ( $V_{\text{run}} > 30 \text{ km s}^{-1}$ ), the effect of the halo potential on the runaway trajectory can be safely neglected at low halo masses, but it may have a modest effect at the highest masses we consider.

an ionizing luminosity-stellar mass relation,  $Q(m)$ , by combining the stellar interior models of Schaller et al. (1992) with the stellar spectral library of Smith et al. (2002) at  $0.05Z_{\odot}$ . We then use the main-sequence lifetime-mass relation,  $t_H(m)$ , presented in Ekström et al. (2011) for their rotating stellar models. At fixed mass, the main sequence lifetime varies by  $\pm 20\%$  depending on the modeling of the stellar interiors and metallicity (Marigo et al. 2001; Schaerer 2002; Ekström et al. 2011).

The second mechanism we consider is the supernova origin of runaways. In this scenario the runaway was at some point in a binary with a more massive companion. When the companion explodes, the surviving star inherits some fraction of the pre-explosion orbital velocity. As in the previous scenario, we specify the fraction of runaways,  $f_{\text{run}}$ , produced in this way. In addition, we must specify the distribution of mass ratios,  $q \equiv M_2/M_1$ , which we assume to be flat over the range  $0.1 < q < 1.0$ , consistent with constraints from the Galaxy (Sana & Evans 2011). We also assume that the primary mass,  $M_1$  is drawn from a Salpeter (1955) initial mass function. Calculation of the runaway velocity requires knowledge of the period distribution, initial-final mass relation for the more massive companion, and, for binaries that remain bound, knowledge of the post-explosion orbital properties (Gott 1972). Consideration of these factors is beyond the scope of the present work (see e.g., Portegies Zwart 2000; Eldridge et al. 2011). Instead, we take an approach that is similar to our treatment of  $V_{\text{run}}$  in the dynamical model: we simply consider a fixed value of  $V_{\text{run}}$  that is similar to the observed average runaway velocity of Galactic O stars.

The supernova mechanism differs from the dynamical mechanism in at least two important respects. First, the lifetime of a runaway is shorter in the supernova scenario because the runaway is formed only after the death of a more massive companion, while in the dynamical scenario the velocity kick is imparted at birth. As we will see below, this effect can be significant. The ratio in median runaway lifetimes between the two mechanisms is  $\sim 3$ , so runaways produced via close dynamical encounters can have a substantially larger impact on  $f_{\text{esc}}$ . In reality, runaways formed in the dynamical channel will be born some finite time after their birth, tempering this difference. The second distinction is that the runaway ionizing LFs are different in the two models. While in the dynamical model runaways have the same LF as the non-runaways, in the supernova model the runaway LF is determined by a combination of the IMF, main sequence lifetime-stellar mass relation, and binary properties. In practice, the supernova runaway LF is not very different from the dynamical runaway LF — it is approximately a power-law with an index of  $\sim -1.7$ .

Both of these models are implemented via Monte Carlo simulations. For our fiducial model we adopt the dynamical mechanism for runaways with  $f_{\text{run}} = 0.3$ ,  $V_{\text{run}} = 60 \text{ km s}^{-1}$ , and  $M_{\text{max}} = 100 M_{\odot}$ . In addition to this fiducial model, a variety of model permutations will be considered in §3.

### 2.3.1. Runaways at High Redshift

We have adopted runaway models based on observations of massive stars in the Galaxy, so it is reasonable to ask whether the population may be different at high redshift. For both the dynamical and the supernova model, the binary population affects the runaway fraction, with more binaries leading to more runaways. High-mass binary formation may be an inevitable consequence of disk fragmentation driven by high accretion rates (Kratter et al. 2010). Indeed, recent simulations

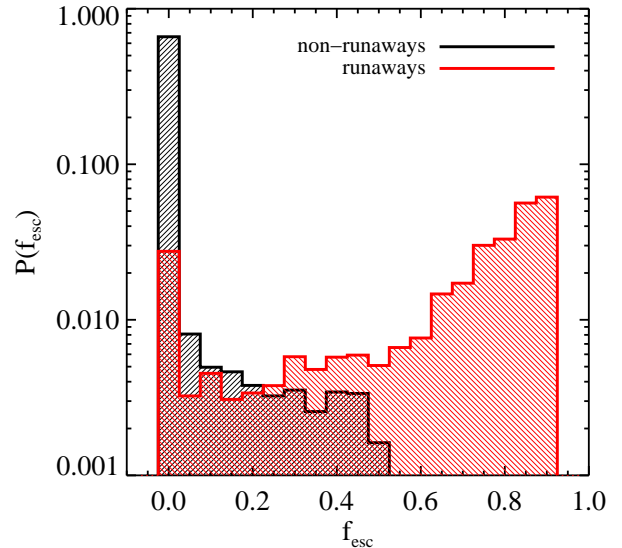


FIG. 1.— Distribution of ionizing escape fractions for individual massive stars in the fiducial model for  $M_{\text{halo}} = 10^8 M_{\odot}$ . The non-runaways (black) and runaways (red) are shown separately.

of population III star formation suggest that binaries may be ubiquitous even in zero metallicity systems (Turk et al. 2009; Greif et al. 2011). It is therefore plausible to assume that the binary fraction at high redshift is similar to that found in the local universe.

In the dynamical ejection model the number of runaways depends on star cluster properties. Following Fujii & Portegies Zwart (2011), who suggest that clusters produce a fixed number of runaways independent of cluster mass, one expects the runaway fraction to scale inversely with cluster mass. Therefore, if more stars are born in smaller- $N$  clusters, a higher fraction will be runaways. Simple estimates of the characteristic fragmentation mass,  $M_c$ , in a  $Q = 1$  disk (Toomre 1964) suggest that it should be smaller at high redshift. In a gaseous disk  $M_c$  scales as  $M_c \sim \Sigma \sigma^2 / \kappa^2$  where  $\Sigma$  is the mass surface density,  $\sigma$  is the velocity dispersion in the gas, and  $\kappa$  is the epicyclic frequency. Adopting Keplerian rotation and using Equations 1 and 2 yields  $M_c \sim \sigma^3 (1+z)^{-3/2}$ . Unless  $\sigma$  is considerably higher in high-redshift disks compared to the Galaxy, we expect  $M_c$  to be lower at high redshift. Everything else being equal, this would suggest that the runaway fraction may increase with redshift. However, the efficiency of producing runaways must decline for the lowest cluster masses, where the number of high mass stars that can form is limited by the cluster mass.

Given all these considerations, we believe that adopting a minimal model, where the runaway fraction does not evolve to high redshift, is acceptable.

## 3. RESULTS

Using the models described above we calculate both the distribution of  $f_{\text{esc}}$  values for massive stars in a given galaxy as well as the galaxy-averaged  $f_{\text{esc}}$  for a range of halo masses. We begin with the results from our fiducial model, and then explore the dependencies of  $f_{\text{esc}}$  on a variety of parameter choices.

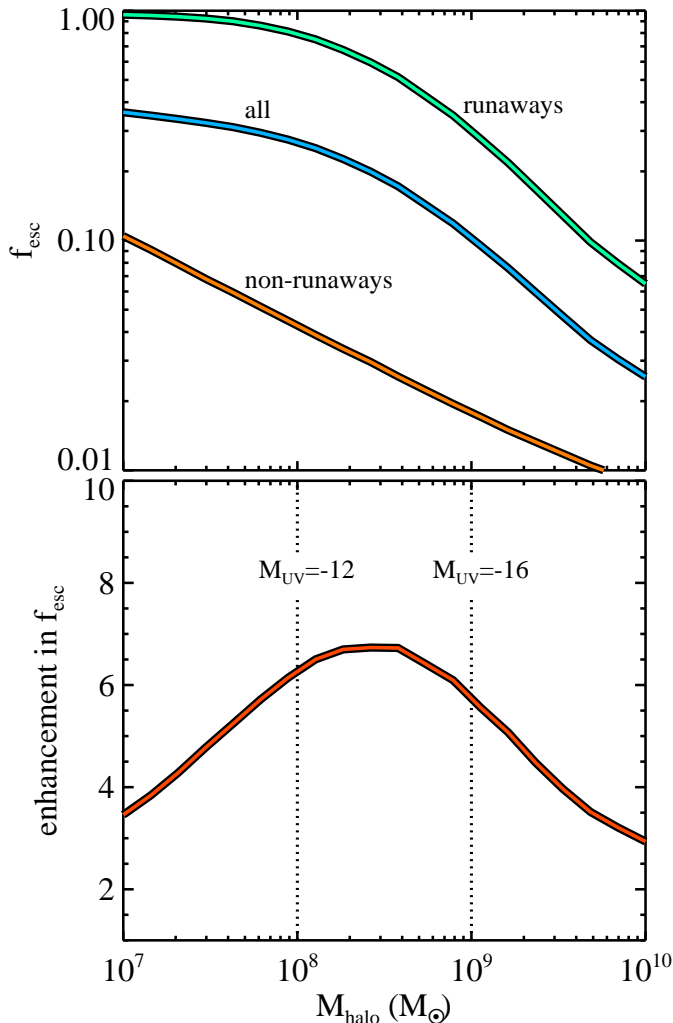


FIG. 2.— *Top Panel*: Escape fraction of ionizing radiation,  $f_{\text{esc}}$ , as a function of halo mass,  $M_{\text{halo}}$ , for our fiducial set of model parameters. The escape fraction is shown for all stars, runaways only, and non-runaways only. *Bottom Panel*: The enhancement in  $f_{\text{esc}}$ , defined as the ratio between the escape fractions computed with all stars and with non-runaways only. Vertical lines represent the approximate halo masses of galaxies with an absolute UV magnitude of -12 and -16 (Kuhlen & Faucher-Giguere 2012).

### 3.1. Fiducial Model

We show the distribution of  $f_{\text{esc}}$  values for stars in our fiducial model in Figure 1 for both runaways and non-runaways at a halo mass of  $10^8 M_{\odot}$ . The vast majority of non-runaways have  $f_{\text{esc}} = 0.0$ , with only a few percent in the “translucent” regime where  $0 < f_{\text{esc}} < 1$  (see also Gnedin et al. 2008). In contrast, a significant fraction of runaways have very high  $f_{\text{esc}}$ , with  $\approx 50\%$  having  $f_{\text{esc}} > 0.6$ . No stars have  $f_{\text{esc}} = 1.0$ . This is because stars are never infinitely far from the galaxy, so the galaxy always occupies a non-zero solid angle capable of absorbing some ionizing radiation.

Figure 2 contains the main result of this paper. The top panel shows  $f_{\text{esc}}$  as a function of  $M_{\text{halo}}$  both for the galaxy as a whole and separately for the runaways and non-runaways. The escape fraction for non-runaways is  $< 3\%$  for  $M_{\text{halo}} > 10^8 M_{\odot}$ , in agreement with previous analytic models of galaxies at  $z = 10$  (Wood & Loeb 2000). For non-runaways,  $f_{\text{esc}}$  increases toward lower masses because the ratio of surface area to volume increases toward smaller galaxies ( $f_{\text{esc}} \propto r_g^{-1}$

for non-runaways). The escape fraction for runaways, however, is always larger than for non-runaways, and approaches unity for the smallest galaxies (recall that  $r_g \propto M_{\text{halo}}^{1/3}$ , making the distance traveled by runaways in low mass halos a larger fraction of the galaxy size).

The bottom panel in Figure 2 shows the ratio between the overall escape fraction and the non-runaway value, which we call the enhancement factor in  $f_{\text{esc}}$ . The turnover at  $M_{\text{halo}} > 10^8 M_{\odot}$  is due to the fact that runaways travel on average a fixed physical distance that becomes a smaller fraction of the galaxy scale radius at larger masses. At sufficiently large scale radii the runaway escape fraction should converge to the non-runaway value, as the runaways will travel an insignificant fraction of a scale length. The runaway  $f_{\text{esc}}$  must therefore decrease more rapidly than the non-runaway value. The enhancement factor has a maximum because  $f_{\text{esc}}$  for runaways begins to saturate near  $M_{\text{halo}} = 10^8 M_{\odot}$ . At lower masses  $f_{\text{esc}}$  for non-runaways continues to increase, so the ratio of  $f_{\text{esc}}$  between all stars and non-runaways decreases at  $M_{\text{halo}} < 10^8 M_{\odot}$ .

In this figure we also label approximate UV magnitudes of galaxies in halos of masses  $10^8 M_{\odot}$  and  $10^9 M_{\odot}$  at  $z = 10$  based on estimates of the  $z = 10$  UV LF (Kuhlen & Faucher-Giguere 2012). These estimates are highly uncertain; they are included here merely to indicate the types of galaxies one might expect to occupy these halos at high redshift.

The key result is that  $f_{\text{esc}}$  increases by factors of 2–8 for  $10^7 M_{\odot} < M_{\text{halo}} < 10^{10} M_{\odot}$  when runaways are included in the model. Figure 2 demonstrates that, in our model, runaways contribute 50–90% of all the ionizing photons that escape from the galaxy. Runaways may therefore play an important role in reionizing the universe.

### 3.2. Model Dependencies

The sensitivity of these results to the assumptions of the model is explored in Figure 3. In this figure we vary the adopted redshift from  $8 < z < 12$ , the dust attenuation, the minimum and maximum stellar mass, the adopted gas density profile,  $n(r)$ ,  $V_{\text{run}}$ , and the ionizing LF. We also explore the predictions of the supernova mechanism for the production of runaways.

The trends are straightforward to interpret. At higher redshift, galaxies are smaller at fixed mass. As the size of the galaxy decreases the effect of runaways becomes stronger both because it is easier for runaways to move to regions of low column density and because, at fixed galaxy mass, smaller sizes result in denser galaxies, lowering the escape fraction for non-runaways (Wood & Loeb 2000). For example, between  $z = 8$  and  $z = 12$   $f_{\text{esc}}$  increases by 70% at  $M_{\text{halo}} = 10^9 M_{\odot}$ .

Increasing  $V_{\text{run}}$  also results in runaways having a greater effect on  $f_{\text{esc}}$ . In this figure we have also considered distributions of  $V_{\text{run}}$ , rather than single values. We have included both a power-law distribution with an index of  $-1$  and a mean of  $40 \text{ km s}^{-1}$ , and a Maxwellian with a dispersion of  $30 \text{ km s}^{-1}$ . In the latter model we have simultaneously set  $f_{\text{run}} = 0.46$  in order to mimic the observational constraints on the runaway population determined by Stone (1991). Adopting a distribution of  $V_{\text{run}}$  rather than a fixed value has a modest effect on the results.

Dust has a very minor effect on the derived  $f_{\text{esc}}$  values. As pointed out by Gnedin et al. (2008), even without dust the vast majority of non-runaways already have  $f_{\text{esc}} = 0.0$  (see Figure

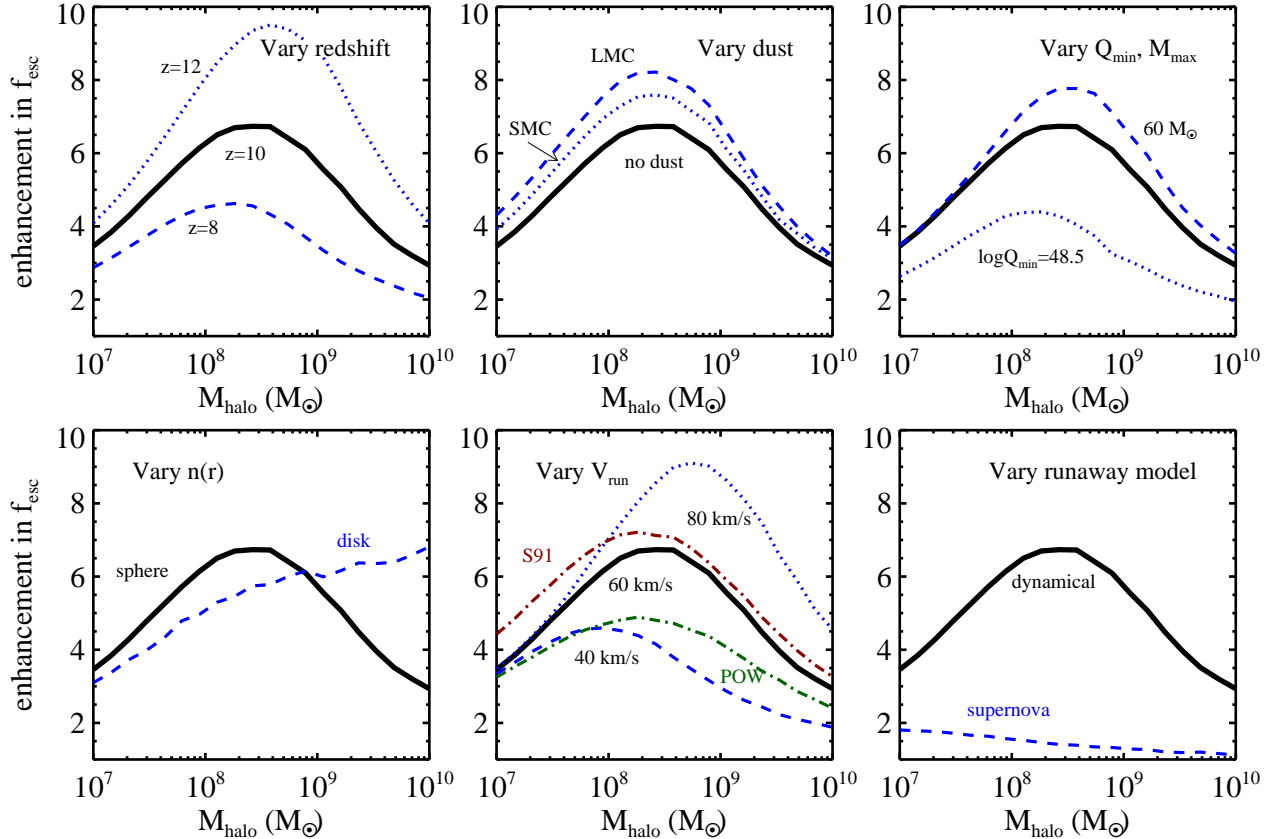


FIG. 3.— The effect of various model parameters and assumptions on the derived enhancement in  $f_{\text{esc}}$  due to runaway stars. The solid line in each panel is our fiducial model where runaways are produced by dynamical encounters. *Top Left*: Variation in the redshift of the model from  $8 < z < 12$ . *Top Middle*: Variation in the treatment of dust. *Top Right*: Variation in the maximum stellar masses of the runaways and in the minimum ionizing luminosity,  $Q_{\text{min}}$ , of the combined runaway and non-runaway population. In the fiducial model,  $M_{\text{max}} = 100 M_{\odot}$  and  $\log(Q_{\text{min}}) = 48.0$ . *Bottom Left*: Variation in the gas density profile. The fiducial model of a spherical exponential profile is contrasted with an exponential disk with a Gaussian vertical density distribution. The disk model has a scale height-to-scale length ratio of 0.2 at  $M_{\text{halo}} = 10^8 M_{\odot}$  and varies as  $M^{-2/3}$ . *Bottom Middle*: Variation in the treatment of the runaway velocities,  $V_{\text{run}}$ . A fixed  $V_{\text{run}}$  is varied from 40–80  $\text{km s}^{-1}$ . In addition, we consider a power-law distribution of  $V_{\text{run}}$  (labelled “POW” in the figure), and a Maxwellian distribution of  $V_{\text{run}}$  as advocated in Stone (1991, labelled “S91” in the figure). In this last case  $f_{\text{run}} = 0.46$ , as advocated by Stone. *Bottom Right*: Variation in the runaway model between our fiducial dynamical model and the supernova model. See the text for details.

1), and so the addition of dust attenuation provides a minor modulation to the source-averaged  $f_{\text{esc}}$ . In addition, the majority of runaways reside in regions of very low column density, where dust attenuation also has a minor effect.

The adopted gas density profile has a dramatic effect on the resulting enhancement factor. In Figure 3 we show results for both a spherical exponential distribution and an exponential disk with a Gaussian vertical distribution. Recall that in our disk model, the scale height-to-scale length ratio varies as  $M^{-2/3}$ , as expected for an isothermal disk, with a value of 0.2 at  $M_{\text{halo}} = 10^8 M_{\odot}$ . In the case of disks, the runaway escape fractions are very high at high masses ( $f_{\text{esc}} \gtrsim 50\%$ ) because the disks are thin and runaways can easily escape in the direction perpendicular to the disk. At fixed mass, the enhancement in  $f_{\text{esc}}$  is a strong function of  $z_g/r_g$ , with smaller values resulting in larger enhancements. At small masses the scale height-to-scale length ratio approaches unity in our model, and so the disks are essentially spheres. Thus the enhancement factor is similar between the two geometries<sup>3</sup>.

Reducing the maximum stellar mass of runaways from

$100 M_{\odot}$  to  $60 M_{\odot}$  causes a modest increase in the runaway enhancement because the mean stellar lifetime of runaways increases as the mass decreases. The runaways are therefore capable of traveling further from the central regions of the galaxy before they explode. We have assumed here that the runaway fraction does not depend on stellar mass at  $> 60 M_{\odot}$ . This assumption is supported by the results of Stone (1991), who finds no variation in  $f_{\text{run}}$  amongst the O-type stars. When the minimum  $Q$  for both the runaways and non-runaways increases from 48.0 to 48.5, the decrease in the mean lifetime of the runaways results in a lower enhancement in  $f_{\text{esc}}$ .

The bottom right panel of Figure 2 shows the effect of adopting the supernova model for runaways rather than the dynamical mechanism. Supernova-produced runaways result in a very modest enhancement in  $f_{\text{esc}}$ . The primary difference between these mechanisms, as implemented herein, is the different lifetime of the runaways. Dynamically-created runaways travel for roughly three times longer than supernova-created runaways, and so the former can more easily reach lower column densities in the galaxy. Observations favor

<sup>3</sup> The enhancement factors are not identical even at the lowest masses be-

cause a sphere is not identical to a disk with  $z_g/r_g \approx 1$ .

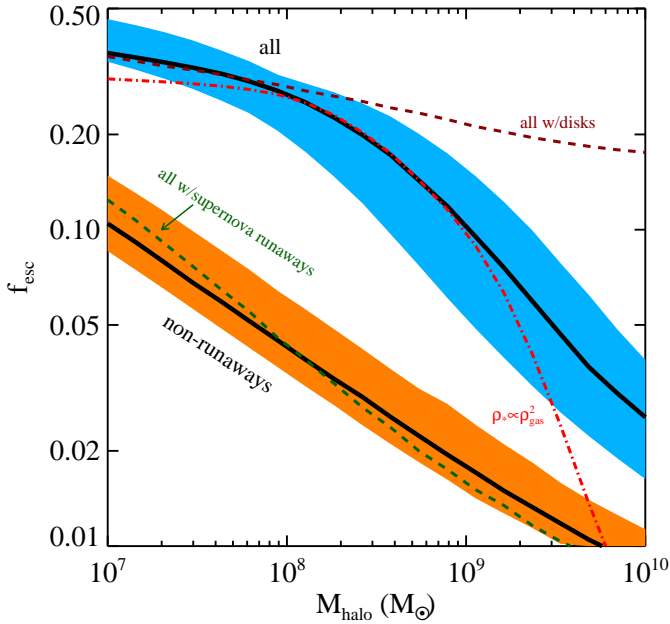


FIG. 4.— Variation in  $f_{\text{esc}}$  between all models considered in the text. The shaded regions encompass the maximum range of the models both with and without the inclusion of runaways (labeled “all” and “non-runaways” in the figure). Thick black lines represent the fiducial model. We have separately plotted the models that deviate substantially from the general trend, including models with a disk geometry, with supernova runaways, and with the stellar density profile scaling as the gas density squared.

roughly equal contributions from dynamically-produced and supernova-produced runaways, and so we can expect reality to lie in between these two extremes. Various stellar evolution models that predict different lifetimes for massive stars should change  $f_{\text{esc}}$  by a more modest factor.

There are additional parameters, not explicitly shown in Figure 2, that can also have a large impact on the enhancement in  $f_{\text{esc}}$ . The runaway fraction,  $f_{\text{run}}$ , clearly will have a direct (linear) effect on  $f_{\text{esc}}$ . The galaxy size also has a strong effect on the results, as can be inferred from the upper left panel of Figure 2. In this panel we consider variation in the adopted redshift, but this is simply changing the galaxy size at fixed mass (see Equation 1). The variation in redshift amounts to only a  $\pm 20\%$  change in the typical size of a galaxy at fixed mass, implying that the results do depend sensitively on size. This highlights the need for incorporation of runaways into realistic simulations of high-redshift galaxy formation to assess their effect on  $f_{\text{esc}}$  in a more quantitative manner.

In Figure 4 we show  $f_{\text{esc}}$  as a function of  $M_{\text{halo}}$  for the full range of models discussed in this section. The shaded regions encompass the total variation in  $f_{\text{esc}}$  due to the different model assumptions. Results are shown both with and without the inclusion of runaways. In the case where runaways are included, we separately highlight the most deviant models. These models are the disk geometry model and the supernova mechanism for the creation of runaways. In the disk model,  $f_{\text{esc}}$  is much higher than the fiducial model at high masses because runaways can more easily escape the galaxy when traveling perpendicular to the disk. In the supernova runaway model  $f_{\text{esc}}$  is considerably smaller because runaways travel for a relatively short time before they explode. In all cases where runaways are produced via dynamical encounters the escape

fraction can be quite high even in moderately large halos.

Finally, in Figure 4 we separately show a model where the stellar distribution is proportional to the gas density squared, in contrast to our fiducial model where the stellar density is linearly proportional to the gas density. This model takes into account that stars form preferentially at the highest densities. In this model the escape fraction for non-runaways is 10–20 times lower than our fiducial model, as the stars are now much more embedded on average. On the contrary, the escape fraction of runaways is identical to the fiducial model for  $M_{\text{halo}} \lesssim 10^9 M_{\odot}$ . In larger halos the galaxy size becomes comparable to, and eventually larger than, the mean distance traveled by runaways, and so the birth environment of the runaways becomes increasingly important in determining  $f_{\text{esc}}$ . Since the non-runaway  $f_{\text{esc}}$  is so much smaller than the runaway  $f_{\text{esc}}$  in this model, the behavior of the runaways entirely determines the behavior of the overall escape fraction. As is clear from Figure 4, this model produces very similar overall  $f_{\text{esc}}$  values for  $M \lesssim 10^9 M_{\odot}$  compared to the fiducial model. At higher masses this model produces lower escape fractions because the runaways are closer to their birth environment (in units of scale lengths), and born in denser regions on average when  $\rho_* \propto \rho_g^2$ .

#### 4. DISCUSSION & CONCLUSIONS

In this paper we have shown that the ionizing radiation from runaway stars may contribute substantially to the reionization of the universe. These stars migrate toward the low-density outer regions of high-redshift galaxies where their radiation can easily escape into the IGM. The importance of their migration is enhanced at high redshift because the galaxies are much smaller than at  $z = 0$  (by a factor of  $\sim (1+z)^{-1}$ ). Assuming that runaways have a prevalence that is similar to what is observed in the Galaxy ( $\sim 30\%$  for massive stars) and that dynamically-created runaways constitute a significant fraction of all runaways, they can increase the total escape fraction of ionizing photons from high-redshift galaxies by factors of 2–8 compared to the escape fraction of non-runaway stars.

Our conclusions depend strongly on three model ingredients: the size of the galaxy, the runaway fraction,  $f_{\text{run}}$ , and the production mechanism for runaways. The effect of runaways on  $f_{\text{esc}}$  depends linearly on  $f_{\text{run}}$ , and therefore if the fraction of runaways is substantially smaller than what we have assumed here, their importance in an extragalactic context will be limited. We have also assumed that galaxy sizes at high redshift scale with halo size in a manner similar to what is found at  $z = 0$ , and so high-redshift galaxies are assumed to be much smaller than local galaxies. Small galaxies strongly enhance the effect of runaways on  $f_{\text{esc}}$ . Finally, we have shown that runaways produced via dynamical encounters have a much larger effect on  $f_{\text{esc}}$  than runaways produced via an explosion of a close companion because of the different runaway lifetimes implied by these models. Observations of runaways in the Galaxy favor a mixture of these two mechanisms (Tetzlaff et al. 2011), and so we can expect that runaways in high-redshift galaxies will play an important role in the escape of ionizing radiation.

The relative importance of runaways depends on the escape fraction of non-runaway stars. In our model the non-runaways have  $f_{\text{esc}} < 10\%$ , and so runaways can be very influential. However, if the non-runaway escape fraction were much higher, then the runaways would necessarily have a diminished impact. As mentioned in the

Introduction, some recent hydrodynamic simulations have found very high escape fractions in high-redshift galaxies (Wise & Cen 2009; Razoumov & Sommer-Larsen 2010; Yajima et al. 2011). These models invoke very efficient feedback that leads to a highly porous ISM which in turn allows for many unobscured sight-lines to massive stars (see also Wood & Loeb 2000; Fernandez & Shull 2011). If these numerical models are correct, then the influence of runaways on  $f_{\text{esc}}$  will be significantly decreased. To better understand the influence of runaways on realistic galaxies, they must be included self-consistently in detailed hydrodynamic simulations that include the effects of radiative transfer.

The influence of runaways on  $f_{\text{esc}}$  can also be tested directly with observations of high-redshift galaxies. If the escape fraction of non-runaways is indeed low, then there will be significant luminosity from recombination emission lines associated with the gaseous disk. Beyond a few disk scale lengths the runaways will dominate the stellar emission, which implies a decrease in the ratio of recombination line flux to ultraviolet flux. In other words, the scale length of a galaxy measured in recombination lines should be smaller than the scale length measured in broadband ultraviolet flux. Such an observation would provide evidence for the influence of runaways (although we note that other explanations for a varying recombination line-to-ultraviolet flux ratio have been proposed, see e.g., Lee et al. 2009). The ratio of scale lengths of the runaways to non-runaways is a decreasing function of halo mass: at  $M_{\text{halo}} = 10^8 M_{\odot}$  the ratio of scale lengths is 2.6 while at  $M_{\text{halo}} = 10^9 M_{\odot}$  the ratio is 1.5, for our fiducial model. Such measurements should be within reach of the next generation

of thirty-meter telescopes. In addition, the occurrence of supernovae far from the inner regions of high-redshift galaxies should be common, and would provide another diagnostic of the prevalence of runaways during the reionization epoch.

Runaways may have other important effects on the evolution of galaxies and the IGM. Ceverino & Klypin (2009) included runaways in a high-resolution simulation of a Milky Way-like disk galaxy and found that they lead to much more efficient heating of the ISM. At high redshift, runaways will also be able to effectively heat and enrich the outer regions of halos and the IGM. Binary formation among the first stars may also have an important effect on IGM heating and chemical enrichment via the production of Population III runaways.

In this paper we have offered a plausible mechanism for the efficient escape of ionizing radiation from galaxies during the reionization epoch. Runaways almost certainly exist at high redshift, and their presence will result in an increase in  $f_{\text{esc}}$ . Detailed simulations that incorporate runaways are required in order to make more quantitative statements regarding their potentially fundamental role in the reionization of the universe. Our results also highlight the need for more detailed observations of the runaway population in the local universe, including the dependence of  $f_{\text{run}}$  on stellar mass, the runaway velocity distribution, and the relative contribution of dynamically-produced and supernova-produced runaways. Fortunately, a wealth of new data on runaway stars should be available in the coming years (e.g., Oey & Lamb 2011; Lamb et al. 2011).

We thank Andrey Kravtsov, Avi Loeb, and Sally Oey for comments on an earlier draft. We also thank the referee for a careful review of this manuscript.

## REFERENCES

- Anosova, J. P. 1986, *Ap&SS*, 124, 217  
 Azimlu, M., Marciniak, R., & Barmby, P. 2011, *AJ*, 142, 139  
 Blaauw, A. 1961, *Bull. Astron. Inst. Netherlands*, 15, 265  
 Bland-Hawthorn, J. & Maloney, P. R. 1999, *ApJ*, 510, L33  
 Bolton, J. S. et al. 2005, *MNRAS*, 357, 1178  
 Bouwens, R. J. et al. 2011a, *ArXiv:1105.203*  
 —. 2011b, *ArXiv:1109.0994*  
 Bryan, G. L. & Norman, M. L. 1998, *ApJ*, 495, 80  
 Bullock, J. S. et al. 2001, *MNRAS*, 321, 559  
 Ceverino, D. & Klypin, A. 2009, *ApJ*, 695, 292  
 Chen, H.-W., Prochaska, J. X., & Gnedin, N. Y. 2007, *ApJ*, 667, L125  
 Clarke, C. & Oey, M. S. 2002, *MNRAS*, 337, 1299  
 Cowie, L. L., Barger, A. J., & Trouille, L. 2009, *ApJ*, 692, 1476  
 Dove, J. B. & Shull, J. M. 1994, *ApJ*, 430, 222  
 Dove, J. B., Shull, J. M., & Ferrara, A. 2000, *ApJ*, 531, 846  
 Dunkley, J. et al. 2009, *ApJS*, 180, 306  
 Ekström, S. et al. 2011, *ArXiv:1110.5049*  
 Eldridge, J. J., Langer, N., & Tout, C. A. 2011, *MNRAS*, 414, 3501  
 Fan, X. et al. 2006, *AJ*, 132, 117  
 Fernandez, E. R. & Shull, J. M. 2011, *ApJ*, 731, 20  
 Fujii, M. S. & Portegies Zwart, S. 2011, *Science*, 334, 1380  
 Fujita, A., Martin, C. L., Mac Low, M.-M., & Abel, T. 2003, *ApJ*, 599, 50  
 Giallongo, E., Cristiani, S., D’Odorico, S., & Fontana, A. 2002, *ApJ*, 568, L9  
 Gies, D. R. 1987, *ApJS*, 64, 545  
 Gies, D. R. & Bolton, C. T. 1986, *ApJS*, 61, 419  
 Gnedin, N. Y., Kravtsov, A. V., & Chen, H.-W. 2008, *ApJ*, 672, 765  
 Gott, III, J. R. 1972, *ApJ*, 173, 227  
 Gott, III, J. R., Gunn, J. E., & Ostriker, J. P. 1970, *ApJ*, 160, L91  
 Greif, T. H. et al. 2011, *ApJ*, 737, 75  
 Grimes, J. P. et al. 2007, *ApJ*, 668, 891  
 Haardt, F. & Madau, P. 2012, *ApJ*, 746, 125  
 Haiman, Z. & Loeb, A. 1997, *ApJ*, 483, 21  
 Heckman, T. M., Sembach, K. R., Meurer, G. R., Leitherer, C., Calzetti, D., & Martin, C. L. 2001, *ApJ*, 558, 56  
 Hoogerwerf, R., de Bruijne, J. H. J., & de Zeeuw, P. T. 2001, *A&A*, 365, 49  
 Inoue, A. K., Iwata, I., & Deharveng, J.-M. 2006, *MNRAS*, 371, L1  
 Iwata, I. et al. 2009, *ApJ*, 692, 1287  
 Kennicutt, Jr., R. C. 1998, *ApJ*, 498, 541  
 Kennicutt, Jr., R. C., Edgar, B. K., & Hodge, P. W. 1989, *ApJ*, 337, 761  
 Komatsu, E. et al. 2011, *ApJS*, 192, 18  
 Kratter, K. M., Matzner, C. D., Krumholz, M. R., & Klein, R. I. 2010, *ApJ*, 708, 1585  
 Kuhlen, M. & Faucher-Giguere, C.-A. 2012, *ArXiv:1201.0757*  
 Lamb, J. B., Oey, M. S., Graus, A. S., & Segura-Cox, D. M. 2011, *ArXiv:1109.6655*  
 Lee, J. C., Gil de Paz, A., Tremonti, C., Kennicutt, Jr., R. C., Salim, S., Bothwell, M., Calzetti, D., Dalcanton, J., Dale, D., Engelbracht, C., Funes, S. J. G., Johnson, B., Sakai, S., Skillman, E., van Zee, L., Walter, F., & Weisz, D. 2009, *ApJ*, 706, 599  
 Leitherer, C., Ferguson, H. C., Heckman, T. M., & Lowenthal, J. D. 1995, *ApJ*, 454, L19  
 Loeb, A. & Barkana, R. 2001, *ARA&A*, 39, 19  
 Madau, P., Haardt, F., & Rees, M. J. 1999, *ApJ*, 514, 648  
 Marigo, P., Girardi, L., Chiosi, C., & Wood, P. R. 2001, *A&A*, 371, 152  
 McKee, C. F. & Williams, J. P. 1997, *ApJ*, 476, 144  
 Mo, H. J., Mao, S., & White, S. D. M. 1998, *MNRAS*, 295, 319  
 Navarro, J. F., Frenk, C. S., & White, S. D. M. 1997, *ApJ*, 490, 493  
 Oey, M. S. & Clarke, C. J. 1998, *AJ*, 115, 1543  
 Oey, M. S. & Lamb, J. B. 2011, *ArXiv:1109.0759*  
 Pawlik, A. H., Milosavljević, M., & Bromm, V. 2011, *ApJ*, 731, 54  
 Pawlik, A. H., Schaye, J., & van Scherpenzeel, E. 2009, *MNRAS*, 394, 1812  
 Pei, Y. C. 1992, *ApJ*, 395, 130  
 Perets, H. B. & Subr, L. 2012, *ArXiv:1202.2356*  
 Pflamm-Altenburg, J. & Kroupa, P. 2010, *MNRAS*, 404, 1564  
 Portegies Zwart, S. F. 2000, *ApJ*, 544, 437  
 Razoumov, A. O. & Sommer-Larsen, J. 2006, *ApJ*, 651, L89  
 —. 2007, *ApJ*, 668, 674  
 —. 2010, *ApJ*, 710, 1239  
 Ricotti, M. 2002, *MNRAS*, 336, L33  
 Ricotti, M., Gnedin, N. Y., & Shull, J. M. 2002, *ApJ*, 575, 49  
 Ricotti, M. & Shull, J. M. 2000, *ApJ*, 542, 548

- Romano-Díaz, E., Choi, J.-H., Shlosman, I., & Trenti, M. 2011, *ApJ*, 738, L19
- Salpeter, E. E. 1955, *ApJ*, 121, 161
- Sana, H. & Evans, C. J. 2011, in *IAU Symposium*, Vol. 272, IAU Symposium, ed. C. Neiner, G. Wade, G. Meynet, & G. Peters, 474–485
- Schaerer, D. 2002, *A&A*, 382, 28
- Schaller, G., Schaerer, D., Meynet, G., & Maeder, A. 1992, *A&AS*, 96, 269
- Shapley, A. E., Steidel, C. C., Pettini, M., Adelberger, K. L., & Erb, D. K. 2006, *ApJ*, 651, 688
- Siana, B. et al. 2007, *ApJ*, 668, 62
- . 2010, *ApJ*, 723, 241
- Smith, L. J., Norris, R. P. F., & Crowther, P. A. 2002, *MNRAS*, 337, 1309
- Srbínovsky, J. A. & Wyithe, J. S. B. 2010, *Publications of the Astronomical Society of Australia*, 27, 110
- Steidel, C. C., Pettini, M., & Adelberger, K. L. 2001, *ApJ*, 546, 665
- Stone, R. C. 1991, *AJ*, 102, 333
- Tetzlaff, N., Neuhäuser, R., & Hohle, M. M. 2011, *MNRAS*, 410, 190
- Toomre, A. 1964, *ApJ*, 139, 1217
- Turk, M. J., Abel, T., & O’Shea, B. 2009, *Science*, 325, 601
- van Zee, L. 2000, *AJ*, 119, 2757
- Whitmore, B. C., Zhang, Q., Leitherer, C., Fall, S. M., Schweizer, F., & Miller, B. W. 1999, *AJ*, 118, 1551
- Wise, J. H. & Cen, R. 2009, *ApJ*, 693, 984
- Wise, J. H., Turk, M. J., Norman, M. L., & Abel, T. 2012, *ApJ*, 745, 50
- Wood, K. & Loeb, A. 2000, *ApJ*, 545, 86
- Yajima, H., Choi, J.-H., & Nagamine, K. 2011, *MNRAS*, 412, 411
- Zwicky, F. 1957, *Morphological astronomy*, ed. Zwicky, F.